Peel performance of composite sandwich parts manufactured by a novel in-situ consolidation robotic 3D printing technique

Samuel Osorio Marino, Dalton Lamoureux, and Kazem Fayazbakhsh*

Department of Aerospace Engineering, Toronto Metropolitan University, Toronto, Ontario M5B2K3, Canada

*Corresponding author: kazem@torontomu.ca; Tel: (+1) 416-979-5000 ext. 556414; fax: (+1) 416-979-5056; https://orcid.org/0000-0003-3963-8282

Abstract

Composite sandwich structures are effective solutions for applications requiring high flexural stiffness and are typically made by bonding skins to a lightweight core using a film adhesive. In this study, a novel in-situ consolidation robotic 3D printing technique is proposed to manufacture thermoplastic sandwich panels. In this process, unidirectional thermoplastic tapes are directly deposited onto a thermoplastic core using a robotic 3D printer. Here, the tapes were low-melt poly aryl ether ketone (LM PAEK) matrix reinforced with continuous carbon fiber (CCF), and the core was separately 3D printed from poly lactic acid (PLA). Pure polymer layers at the top and bottom of the core (zero versus two) and 3D printing speed of the skins (10 versus 5 mm/s) were explored as two independent variables. Two specimens were made for each configuration, and the consolidation strength between the skins and the core was investigated per ASTM D1781 climbing drum peel test. Specimens with two layers of pure PLA 3D printed at 10 mm/s exhibited the highest quality skins with minimal gaps between tapes and no imprint from the core. The normalized average peeling load for all specimens was 84.7 N/cm, which is 182% greater than the baseline value of 30 N/cm.

Keywords:

In-situ consolidation robotic 3D printing, Low-melt poly aryl ether ketone (LM PAEK), Continuous carbon fiber composites, Climbing drum peel

Composites Part A: Applied Science and Manufacturing

https://doi.org/10.1016/j.compositesa.2026.109723

1. Introduction

Composite sandwich structures generally consist of two rigid skins separated by a lightweight core and are efficacious parts in applications requiring low weight and high flexural stiffness. Traditionally, in high-performance applications, the skins are fabricated first from a continuous fiber-reinforced thermoset prepreg and are later bonded to the core by a film adhesive [1]. This conventional technique is a two-step process that requires proper surface preparation prior to sandwich structure construction to ensure high interfacial bond strength and durability [2, 3]. The required surface preparation and quality control along with the separate skin fabrication make the manufacturing process costly, labour intensive, and time-consuming [4]. Furthermore, sandwich structures made from thermoset skins or adhesives are not recyclable [5].

Additive manufacturing (AM), also called 3D printing, has mainly been employed to manufacture thermoplastic cores, while continuous fiber composite skins are still made using traditional fabrication techniques [6-8]. Li and Wang [6] used PolyJet 3D printing and made three core geometries from VeroWhite, and the skins were carbon fiber-reinforced Vinylester. The skins were later bonded to the core using an epoxy adhesive to make three samples for three-point bending test. The truss core sandwich sample provided highest flexural stiffness and strength. Lu et al. [7] 3D printed varying poly lactic acid (PLA) core geometries, namely: bi-grid, tri-grid, quadri-grid, and Kagome-grid. The skins were carbon fiber epoxy-T300 and were bonded to the core using an epoxy resin to manufacture four specimens for three-point bending test. The main failure mechanism for all specimens was core shear failure, though skin-to-core debonding was also present. Alshaer and Harland [8] 3D printed seven core geometries including gyroid from Nylon PA12. They made the skins from carbon fiber and an epoxy resin using a wet lay-up process and then used the same resin to bond the skins to the core to manufacture three-point bending samples. The gyroid core sandwich specimen showed the highest relative normalized ultimate strength, modulus, and bending stiffness. All sandwich specimens suffered from skin-to-core debonding throughout testing, which was attributed to the core's material and inconsistencies during hand lay-up of the composite skins.

Other researchers used 3D printing, specifically material extrusion (MEX), to fabricate thermoplastic sandwich parts in a one-step process. They mainly 3D printed the skins and the core from pure polymers, e.g., PLA [9] or ABS [10], and performed three-point bending tests. However, these 3D printed sandwich panels have limited applications considering their low structural performance. A few researchers 3D printed both the skins and the core from continuous carbon fiber (CCF)-reinforced nylon filaments. Um et al. [11] produced sandwich structure beams with trapezoidal corrugated cores of increasing density and performed three-point bending tests. For comparison, nylon reinforced with CCF and short CF were used for the core while all the skins were 3D printed from nylon-CCF. They found specimens with CCF skins had significantly greater flexural stiffness than those made with short CF. Their manufacturing process still used an epoxy adhesive to bond the skins to the core, making it a two-step process. Sugiyama et al. [12] obviated

the need for the adhesive agent by employing direct thermoplastic-to-thermoplastic consolidation to produce unibody CFRTP sandwich structure specimens in one FFF process. First, the bottom skin was produced by laying five layers of CCF filament in alternating 0° and 90° orientations. Next, twenty layers of filament made up the core with either honeycomb, rhombus, rectangle, or circle repeating-unit cores. Finally, the top skin was produced by laying five layers of filament with the same alternating orientation pattern as the bottom skin. They 3D printed a total of four specimens, one for each core type, and performed three-point bending tests. Typically, tensile failure occurred on the bottom skin of the specimen first, followed by a compressive failure on the top skin. Moreover, interlaminar shear failure was detected within all cores. Nonetheless, debonding of the interface between the skin and the core was not detected, which showed the efficacy of in-situ consolidation as a joining technique.

Previous studies in the literature have focused on three-point bending tests to evaluate mechanical performance of the composite sandwich panels and witnessed frequently skin-to-core debonding throughout testing [7, 8, 11]. Therefore, to increase structural performance of sandwich structures, the bond strength must be improved first. The three-point bending test, however, does not provide a proper representation of the bond strength. Here, the standard climbing drum peel test for adhesives per ASTM D1781-98(2021) can be utilized [13]. In addition, researchers have only investigated 3D printed sandwich panels from pure polymers or low-performance polymers reinforced with continuous fiber. These investigators used 3-axis gantry-based desktop 3D printers that are limited in terms of build volume and manufacturing flexibility. In a previous study [14], we used robotic 3D printing to manufacture tensile samples from low-melt poly aryl ether ketone (LM PAEK) reinforced with CCF. The results showed 32.4% and 79.0% improvement in tensile strength and modulus, respectively, compared with nylon-CCF material from Markforged. Recall that Um et al. [11] and Sugiyama et al. [12] used nylon-CCF in their 3D printed sandwich panels.

In this study, robotic 3D printing is used to deposit CCF prepreg tapes from LM PAEK onto 3D printed PLA cores to manufacture thermoplastic composite sandwich structures. We call this process ‘in-situ consolidation’ since there is no secondary step in the manufacturing process, hence it is in-situ. Furthermore, in our study, the core was 3D printed and already consolidated before depositing the tapes; therefore, there was no significant co-consolidation between the skins and the core. This novel in-situ consolidation process removes the need for the film adhesive in the sandwich structure and extensive surface preparation activities. This way, fabrication cost and time are reduced while simultaneously, the recyclability of final parts is improved. Furthermore, the degree of consolidation between the core and the skins is evaluated using climbing drum peel test, which has not been investigated for 3D printed sandwich structures so far.

The current study evaluates peeling performance of in-situ consolidated thermoplastic sandwich specimens according to a modified ASTM D1781 test standard for climbing drum peel. Section 2 describes the methodology including specimen design and manufacturing and testing apparatus

and procedure. Section 3 illustrates specimens before and after testing and provides peeling load values along with difficulties encountered during manufacturing and testing. This paper concludes with major findings, research limitations, and directions for future work.

2. Methodology

This chapter describes the design, manufacturing, and testing of thermoplastic sandwich structures fabricated using in-situ consolidation robotic 3D printing process.

2.1. Specimen design

The specimen per ASTM D1781 is 76 mm (3 in.) wide, w, and at least 305 mm (12 in.) long, l_{total}. The length includes 25.4 mm (1 in.) overhangs, l_{clamp} on one facing at each end of the specimen to allow clamping (Figure 1). The standard does not require any specific specimen thickness so long as no bending is present while testing, ensuring that peeling is the only type of load being applied [13].

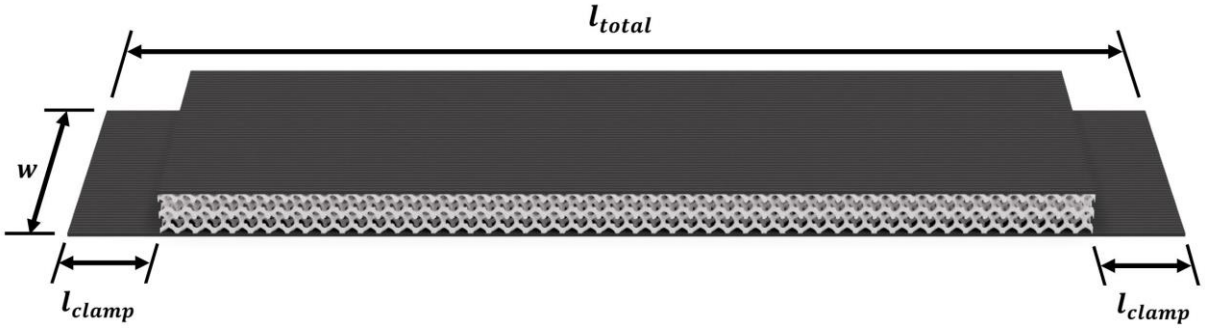

Figure 1. Specimen dimensions per ASTM D1781.

In this work, the specimen length of 305 mm was reduced to 255.8 mm including two unmodified 25.4 mm overhangs because of limited crosshead displacement in the testing apparatus. The length of the region of peeling (not including the overhangs) was therefore 205 mm. Furthermore, due to limited LM PAEK-CCF prepreg tape feedstock, the core width was reduced to 20 mm to allow for deposition of three tapes with a width of 6.35 mm before consolidation. A nominal core thickness of 5 mm was chosen based on preliminary investigation demonstrating that it is sufficient in preventing bending of the specimen during testing. The modified specimen length still provides a peeling distance of about 126 mm, which is very close to the 127 mm value required in the standard [13]. Therefore, the specimen design should provide accurate evaluation of the interfacial strength between the skins and the core.

The core was designed to include the portion of the skin overhangs, called overhang tabs. This allowed for fixing the specimen to the build platform by taping the overhang tabs using Kapton® 100 µm PI tape to the build platform. During the skins' 3D printing, LM PAEK-CCF tapes were deposited on top of the core including the overhang tabs covered with the Kapton® tape, which prevented consolidation of the skins to the core in the overhang areas. This way, the core overhang

tabs were easily broken off, resulting in a clean skin laminate overhang on both sides of the specimen. This technique is similar to what other researchers used to form a beginning of crack propagation for mandrel peel testing [15]. In addition, six outer tabs were printed along both lengthwise edges of the cores for affixing the specimens during the skins' 3D printing. The 3D model and the drawings of the core in Fusion 360 are included in the data repository of this paper.

In-situ consolidation using robotic 3D printing works by depositing thermoplastic prepreg tapes directly onto a 3D printed thermoplastic core. During disposition, the hot nozzle softens the feedstock tape and the core just beneath it, which then cools as it moves along the part. This way, polymer chain entanglement occurs between the two thermoplastics, and the skins and the core consolidate as a one-piece thermoplastic sandwich part. Here, consolidation strength is used to describe the interfacial strength between the skin and core in place of the traditional terminology—bond strength—since a bond implies the usage of a third constituent adhesive.

Increased resin flow and polymer chain entanglement can be enabled by free resin unencumbered by fibers [16]. Integrating layers of pure polymer between the core and the skins results in more evenly distributed interdiffusion of polymer chains, which would increase interfacial strength. Lower cooling rates correlate with stronger consolidation [17, 18], which can be controlled using the 3D printing speed of the skins. At the same time, the deposition speed directly impacts the amount of time the feedstock spends in the heated nozzle during extrusion, thereby inducing a thermal effect. Furthermore, the 3D printing speed determines the production rate, which is an important parameter in automated manufacturing techniques. Note that the suitable nozzle temperature for processing LM PAEK-CCF prepreg tapes was found in our previous work [19] and was used here. Therefore, this study explores the impact of pure polymer layers and the 3D printing speed on the consolidation strength of in-situ consolidated thermoplastic sandwich panels.

Preliminary investigations with one pure polymer layer revealed that it did not retain sufficient rigidity to be considered a firm base for consolidating the skins. When heated, the top layer of the core exhibited bowing wherever it was not supported by the core geometry walls, thus leaving gaps between the tapes and the core like the case with no pure polymer layers. Having two layers of pure polymer rather than one mitigated this issue, and it was not increased further considering the weight penalty. We explored the impact of the 3D printing speed in manufacturing laminates from LM PAEK-CCF in the past and found that both 10 mm/s [19] and 5 mm/s [20] provide high-quality parts. Here, these two 3D printing speeds are used in the test plan. Table 1 lists the four sets of specimens explored in this study. Note that the drum peel specimens are large and their fabrication process is complex. That is why only two specimens per set were considered, to explore top and bottom skins of a sandwich construction. Researchers in the literature, when exploring sandwich composite specimens, also had a limited number of specimens per set, or even a small total number of samples per study [9-12].

Table 1: Test plan and specimen identification.

Specimen ID	Number of Pure PLA layers	Skin Print Speed (mm/s)	Quantity
0L-S10	0	10	2
0L-S5	0	5	2
2L-S10	2	10	2
2L-S5	2	5	2
		Total	8

2.2. Specimen manufacturing

AM™ 200 filament from Victrex is the same PAEK polymer as the prepreg tape used for the skins. However, its processing is much more complex than standard materials like PLA, especially for our core geometry (see Figure 2). Since the aim of this study is to explore in-situ consolidation of sandwich panels and the possibility of the film adhesive removal from the construction, PLA was selected for the core. PLA has a low glass transition temperature (T_g) of 57.2 °C [21] compared to LM PAEK of about 150 °C [14]; therefore, these vastly different T_g values provide a worst-case scenario for in-situ consolidation of the sandwich panels. The cores were manufactured in two sets of four (0L and 2L) from natural PLA (Esun, Guangdong, China) using a Kobra 2 Max 3D printer (Anycubic, Shenzhen, China). The ambient room temperature and relative humidity were 19.4 °C and 15.9%, respectively, during fabrication.

The 3D model of the core was sliced into G-code on UltiMaker Cura 5.1.0. The 3D printing process and design parameters are as follows: flat build orientation, filament diameter of 1.75 mm, layer height of 0.2 mm, bed temperature of 65 °C, nozzle temperature of 210 °C, nozzle diameter of 0.4 mm, 3D printing speed of 80 mm/s, with fan cooling, infill density of 20%, and gyroid infill. The gyroid structure has a high surface-area-to-volume ratio [22] and enhanced flexibility and impact resistance, making it beneficial for parts that undergo bending and require a certain degree of flexibility [23]. For the cores with two pure layers of PLA on the top and bottom sides of the core, ±45° raster angles were used. The infill density of 20% corresponds to a distance between repeating unit cells of 4 mm. The average mass of the PLA cores was measured to be 7.2 g and 11.4 g for 0L versus 2L specimens, respectively (Figure 2).

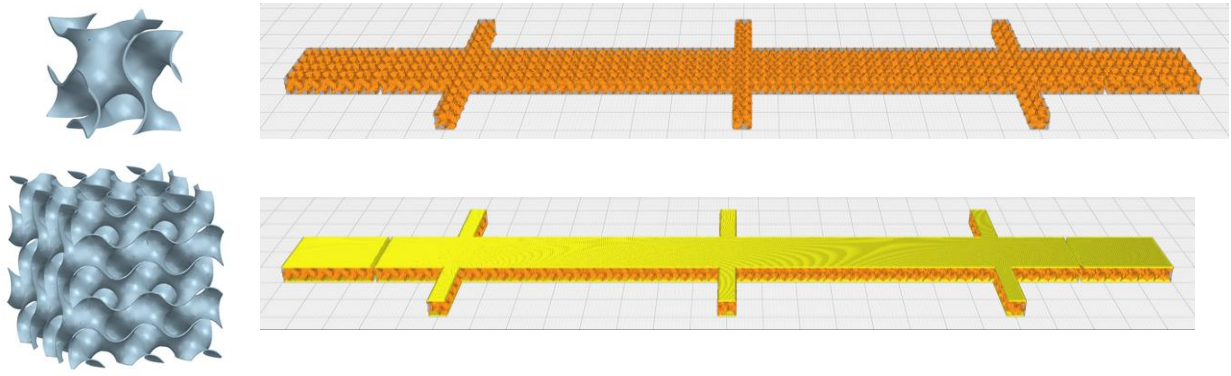

Figure 2. Gyroid unit cell and structure (left top and bottom [24]), Gcode visualization of 0L core and 2L core including two overhang tabs and six outer tabs (right top and bottom).

Robotic 3D printing of LM PAEK-CCF prepreg tapes was performed using the ABB IRB 1200, which has a 0.9 m arm reach and can accommodate a 5 kg payload (Figure 3, left). The set up is similar to our previous studies [14, 20] with a new 3D printing head consisting of aluminum sheets separated by steel spacers for easier manufacturability and heat management. The manufacturing apparatus includes the robotic arm, a programmable logic controller (PLC) box, transformer, IRC5 control unit, build platform, Flexpendant, and a 3D printing head installed. A slotted nozzle (width of 6.6 mm) with two heating elements and one thermocouple inside a copper heating block form the hot end with a cross-section view shown in Figure 3 (right).

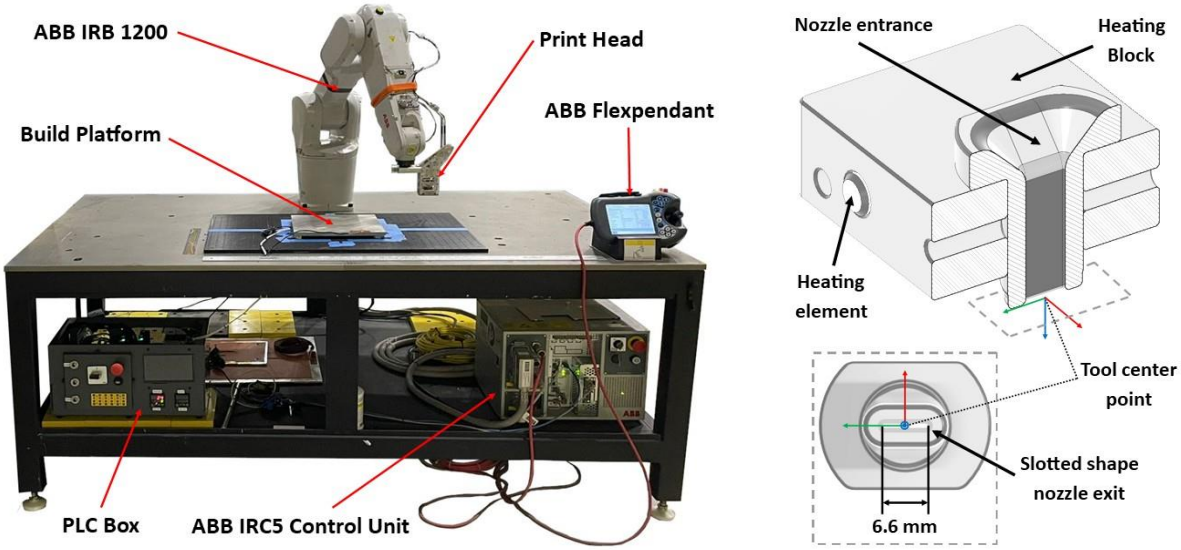

Figure 3. Robotic 3D printing set-up (left) and cross-section of the hot end (right).

ABB RobotStudio 2025.2 was used to graphically program the robot's movement to deposit three tapes side by side in two layers per each side of the core (a total of 12 tapes per specimen). The feedstock is a thermoplastic unidirectional tape (TPUD) with LM PAEK reinforced with HTS45 carbon fiber with a width of 6.35 mm (1/4 in.) and a nominal thickness of 0.14 mm supplied by Teijin Carbon America [25]. The tapes were dried in an MCB(H)-1.2-.33-.33-H/AC MicroClimate chamber (Weiss Technik, Heuchelheim, Germany) at 140 °C for 70 minutes before 3D printing. This drying time was found sufficient based on a thermal gravimetric analysis (TGA) test, and it took the chamber about 14 min at 10 °C/min to reach the soak temperature. A nozzle temperature of 380 °C [19], room temperature for the build platform, and 0° raster angle (along the specimen length) were used for manufacturing.

To 3D print skins without gaps or overlaps between individual tapes, the tape raster offset (TRO) needs to be selected properly. TRO is the distance between the centerlines of two tapes deposited adjacent to each other. It is not equal to the pre-process tape width since the feedstock changes dimensions during deposition due to Poisson effect, orthotropic coefficient of thermal expansion,

and crystallization of the tapes. Based on the results from our previous study [19], we performed a preliminary investigation and 3D printed a one-layer skin on a 60 °C stainless steel build platform with different TROs. We found that a TRO of 6.12 mm between the first and the second tape, and a TRO of 5.92 mm between the second and the third tape produced a skin with almost no gaps and overlaps. A lower TRO value for the third tape deposition was needed considering the difference in boundary conditions between the tape deposited first and second and was described in detail in [19]. A z-height of 0.100 mm above the core was used for 3D printing the first layer of the skins, which was increased to 0.184 mm (the pre-processed tape thickness) for the second layer deposition above the first one. Figure 4 shows the eight 3D printed sandwich specimens for climbing drum peel testing before the final trimming of the overhang skins to 25.4 mm. Visual observations of the specimens revealed higher overall surface quality for specimens having two layers of pure PLA between the skins and core compared to those having none. Those with two layers and printed at 10 mm/s demonstrated minor to no gapping between tapes, smooth surface finish, no stray fibers, and no delamination. Specimens printed at 5 mm/s demonstrated overall narrower tapes.

Figure 4. In-situ consolidated sandwich specimens for climbing drum peel with extended skins.

While TRO values were found to produce skins with no gaps and overlaps in ideal scenarios, a few samples still showed some gaps between the tapes in the skins, especially 0L specimens (e.g., see 0L-S5-1 in Figure 4). The tape deposition onto a core with two pure PLA layers resembled closer a deposition on a steel build platform while a core with no pure PLA layers resulted in more shrinkage in the tape along its width. Furthermore, there are inherent variabilities in the 3D printing

process which create variations among specimens with the same fabrication process parameters. There are manufacturing errors resulting from the robotic arm inaccuracies and the nozzle slot width, which is slightly larger than the tape to prevent nozzle clogging. Figure 5 shows how for a case with a gap between tapes, the hot nozzle presses the tape on the heated PLA core resulting in polymer squeeze-out and a more significant reduction in the tape width. For drum peel testing, consolidation between adjacent tapes is considered irrelevant since the peel force depends on loads acting between the tapes and the core surfaces.

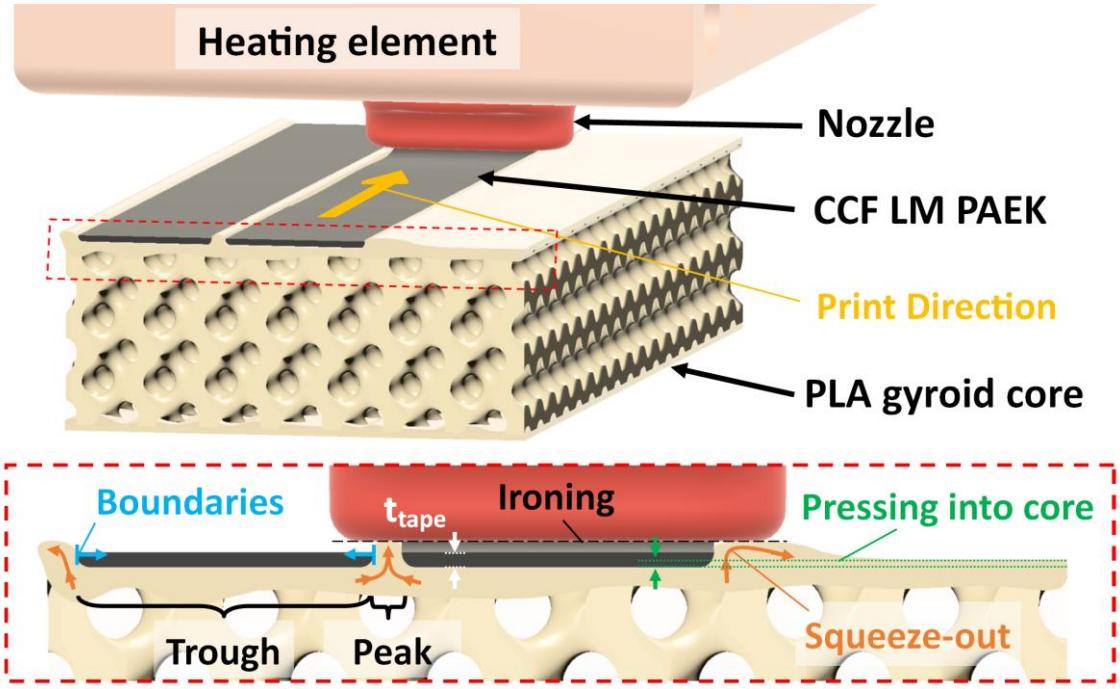

Figure 5. Thermoplastic tape deposition onto a core with a gap between the two tapes.

The side of the core which was on the Kobra 2 Max 3D printer build platform during its fabrication and had a smoother surface was also placed on the build platform of the robotic 3D printer. This way, the first skin of the sandwich specimen was placed on a side of a core which had a rougher surface. This is called “Side A” (SA) for the sandwich specimens and “Side B” (SB) refers to the other side.

2.3. Testing apparatus and procedure

Climbing drum peel for adhesives measures peel resistance as the average steady-state load required to separate the skins from the core over a certain distance. By applying tension in the top clamp, torque is generated in the drum which is then converted to a localized tensile force normal to the specimen’s surface along the line of contact with the drum. As the circular drum rotates and climbs upward, the skin is peeled and is wrapped around it. As the drum rotates and moves upward, the skin is peeled and is wrapped around the circular drum. The fixture was procured from

Wyoming Test Fixture and was mounted on a UTS STM-50 testing machine (United Testing Systems, Concord, Canada) with a 2.22 kN (500 lbf) load cell (Figure 6). The upper portion of the fixture included the load cell along with its insertion point, upper clamp along with its tightening rod, and the pin to secure them together. The lower portion included the flanged drum in which the bottom 25.4 mm overhang (leading edge of peeling) of the specimen was inserted into the drum's clamp and tightened with the tightening rod. The bottom adapter, which connects to the testing machine, was inserted into the mounting point and secured with a pin.

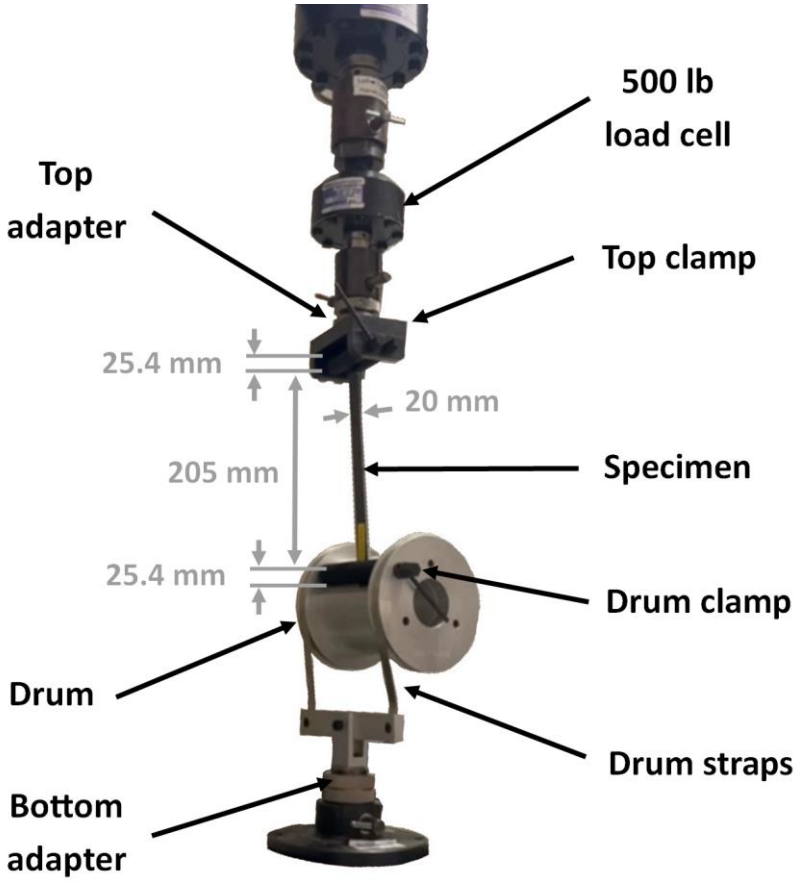

Figure 6. Climbing drum peel test apparatus.

The sandwich structures were manufactured to have skin overhangs on both ends of one of the specimen's faces to clamp the specimen to the tensile testing machine. For each set of specimens, one was tested on Side A (SA) and the other for Side B (SB). The top of the specimen was first secured by inserting the overhang into the top clamp, ensuring it was oriented parallel to the direction of drum climb, and tightening the rod. Next, the top assembly was jogged downward until the bottom overhang of the specimen fell into drum clamp. At this point, drum clamp was tightened. To ensure consistency throughout testing, the bottom overhang for all specimens was the leading edge of the sample where tape deposition started, except for 2L-S10-1 and 2L-S5-1 specimens that required retesting. Then, the upper head was jogged manually upwards to remove

any slack in the loading straps but not enough to begin peeling of the skin off the core. With the drum suspended and some tension in the skin, the load was set to zero before starting the test. The test program was run at a constant crosshead speed of 25.40 mm/min per the ASTM standard. When the testing machine visually appeared to almost reach its displacement limit, the test was stopped. Load versus crosshead displacement data was recorded at 10 Hz frequency.

3. Results and discussion

This section includes dimensional measurements of the in-situ consolidated sandwich specimens along with peeling load values and observations from the specimens after failure. The impact of the core type and the 3D printing speed on the consolidation strength is discussed.

3.1. Dimensional measurements

The thickness of the sandwich specimens was measured using a 3732XFL-1 digital micrometer (Starrett, Athol, USA) in 15 different points within each sample. Measurements for all eight specimens and thickness distribution plots are provided in the data repository. Furthermore, the width of the skins used for testing was measured by a MAXIMUM IP54 caliper (Canadian Tire, Toronto, Canada) at the front and the back of each specimen. Table 2 summarizes the thickness and width measurements based on the core type and the 3D printing speed. The average percent reduction from the nominal thickness of the sandwich specimens is the difference between the average thickness for each set and the nominal thickness for the samples, which equals the thickness of the core and four layers of consolidated prepreg tapes, a total of 5.56 mm.

Specimens with no pure PLA layers had lowest average thickness values among all specimens with about 36% reduction from the expected nominal thickness. They also had the lowest consolidated tape width, with 5 mm/s 3D printing speed exhibiting the narrowest skins. This behavior is expected, as the hot nozzle increases melting of the sparse PLA 0L core, causing the tapes to sink further into it. This mechanism and the polymer squeeze-out was explained in Figure 5, which resulted in gaps between consolidated tapes (see 0L specimens in Figure 4). On the other hand, 2L specimens had highest average thickness and width, with 10 mm/s 3D printing speed showing maximum values. Increased 3D printing speed for 2L-S10 specimens meant lower melting of the PLA core, resulting in maximum thickness and width and no gaps between tapes (see 2L specimens in Figure 4, especially 2L-S10).

Table 2. Average thickness and width values for different specimen sets.

Configuration	Average thickness (mm)	Percent reduction from nominal (%)	Average width (mm)
0L-S10	3.568	36%	17.53
0L-S5	3.593	35%	16.70
2L-S10	5.175	7%	18.50
2L-S5	4.467	20%	18.21

3.2. Peeling load and failure type

Figure 7 shows load versus crosshead movement for all eight specimens along with images showing the specimens after failure. In general, the load-extension curves exhibited an increasing trend prior to the start of peeling. This increasing trend described the tension being applied to the drum straps to remove any remaining slack. Next, a local maximum was identified in each curve which indicated the start of peeling. Initially, a higher load was required to start peeling the skin off the core; thereafter, a drop indicates release after peel initiation. Afterwards, steady peeling begins, and the subsequent force-extension points are included for calculating the average peeling load. The range of test is very similar among all specimens with an average of 31.4 mm crosshead displacement and CV of 8.6%. Only specimens 0L-S5-1 and 2L-S5-2 demonstrated a different test range, which was simply because of different amounts of slack present in the drum straps from the initial mounting.

Theoretically, SA and SB per configuration should have yielded similar results because they were fabricated with the same parameters. The only difference is that SA is 3D printed first on the rough side of the core, and SB is second on the smooth side. Nevertheless, pairs of equivalent configurations showcased some degree of variability in peeling behaviour. Like any other composites manufacturing and testing technique, random effects and errors can create these variations. Here, SA versus SB of the two specimens can be considered a random effect, and variabilities in the robotic 3D printing between the two samples is a random error.

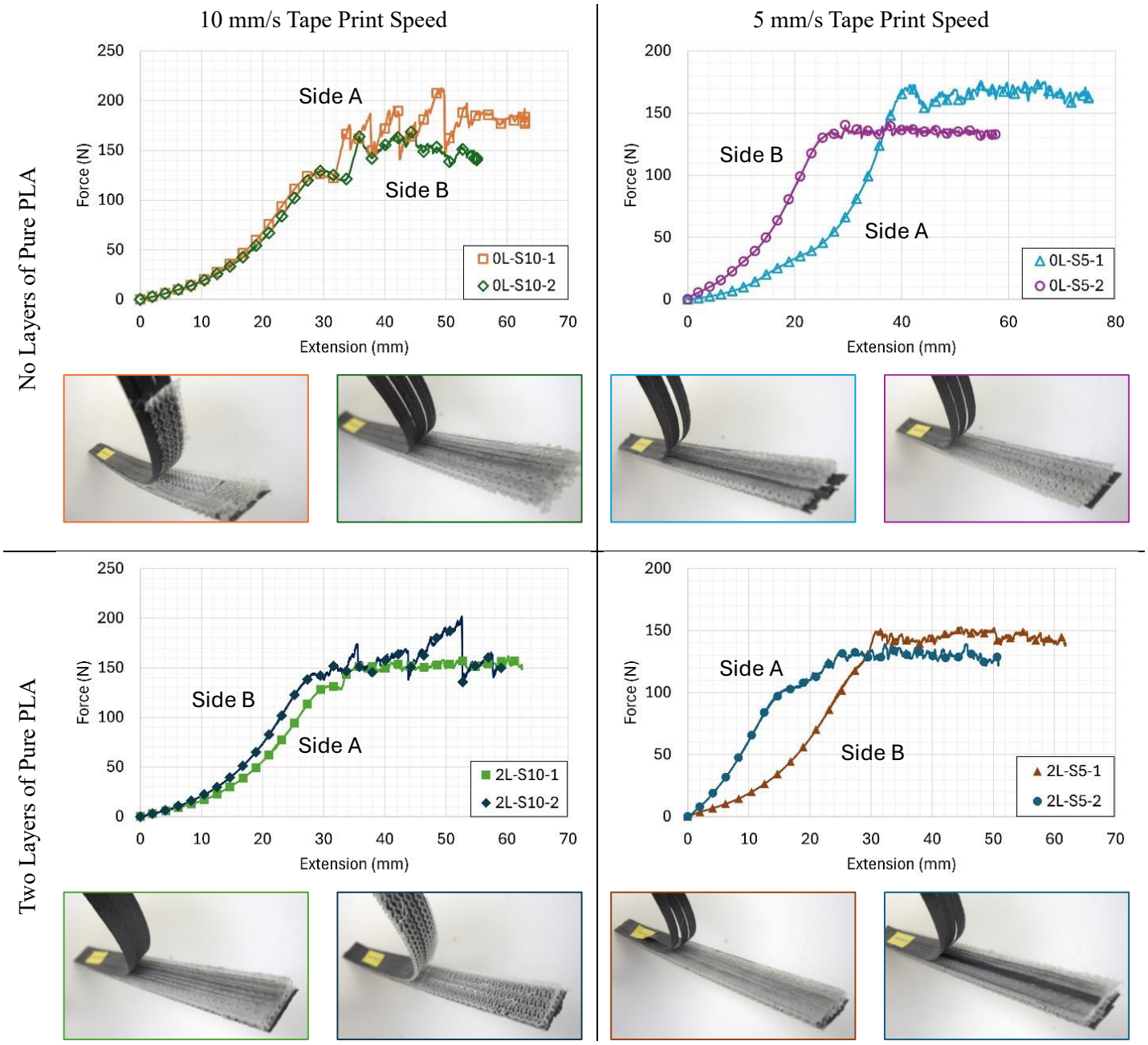

Figure 7. Load versus crosshead movement along with the failure type: core type (rows) and 3D printing speed (columns).

Two specimens exhibited larger degrees of variation along the peel including large peaks and drops, namely 0L-S10-1 (□) and 2L-S10-2 (◆). Both specimens displayed failure within the core rather than at the interface, which is indicative of a stronger consolidation at the interface than within the 20% gyroid infill of the PLA core. FFF 3D printing, due to its layer-wise additive nature, produces anisotropic parts with a low interlayer weld strength. Since peeling is achieved by applying tension perpendicular to the layers, debonding may occur there. Peeling between PLA layers of the core occurred where the raster ran in the 0° direction which is consistent with a

"bridging" phenomenon observed in Figure 8. The tension within a "string" of PLA was enough to strip it from both adjacent PLA z layers yet was not strong enough to cause it to snap immediately. When enough bending was present in the specimen due to the string sustaining the tension, the string fractured. These fractures are observed in the drum peel curves as immediate drops of force.

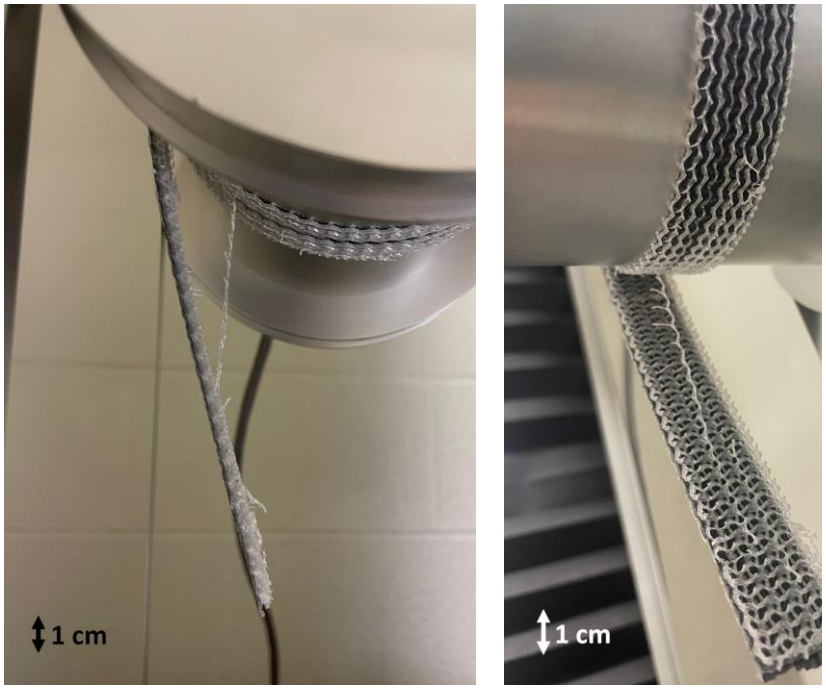

Figure 8. 2L-S10-2 specimen (◆) during testing with failure within the core: side view (left); and close-up front view (right).

The overall interfacial strength is the accumulation of many consolidation points which individually disconnect due to the perpendicular tensile force exerted during peeling. Fibers oriented away from the surface of the core is a proof of tension along individual carbon fibers which eventually snap during peeling (Figure 9). They cause peaks and drops in the load-extension graphs, albeit on a much smaller scale than failure within the core. This phenomenon, although seen throughout all specimens, was more prevalent in a few samples like 0L-S5-1. It is expected that specimens with higher dark residue on the PLA core after testing (meaning more carbon fibers) to have greater skin-to-core consolidation strength.

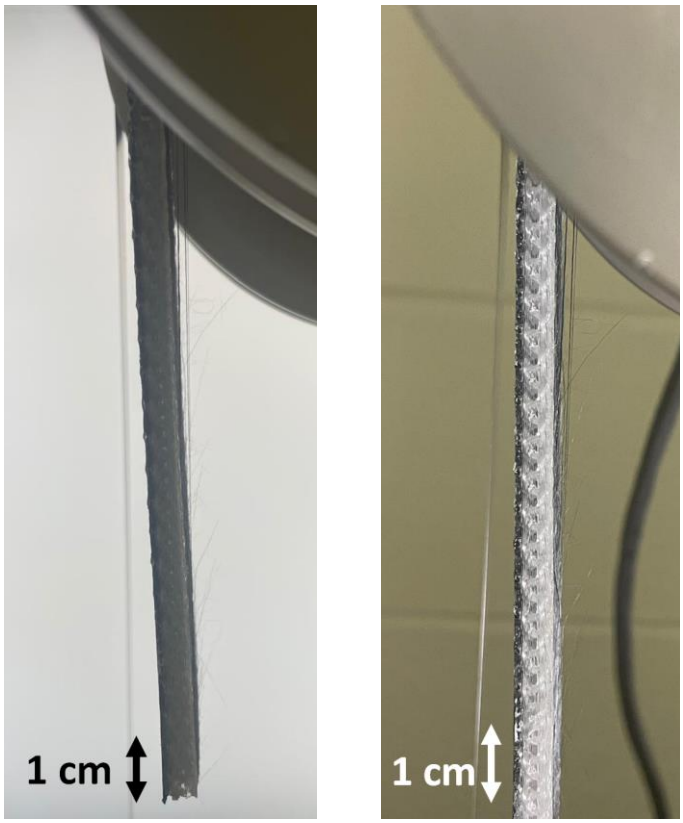

Figure 9. Fibers oriented out of plane of the specimen after the skin peeling: drum reaching top of the specimen (left); and a closer view (right).

Table 3 summarizes the visual observations made for the post-failure specimens. The failure type was one or a combination of peeling between the skin and the core, failure within the core, and delamination within the skin. Visual inspection and caliper measurements of the specimens after testing were used to calculate the area percentage of each failure type. Recall that Figure 7 includes images of all specimens after failure. As an example, specimen 0L-S10-1 shows two failure types: peeling between the skin and the core, and failure within the core. For the former, the black carbon fiber composite facesheet can be observed on the upper part and the white PLA core on the lower part. For failure within the core, the white PLA core can be seen on both sides. Using a caliper, we calculated the area percentage for each failure type and reported it in Table 3. The same procedure was followed for all the remaining specimens. Furthermore, the amount of carbon fiber residue on the PLA core was noted.

Out of the eight specimens, only two exhibited failure within the core (0L-S10-1 and 2L-S10-2). The other six specimens showed mainly peeling between the skin and the core. Interestingly, specimen 0L-S10-1 had a combination of two failure modes.

Table 3. Failure type of the specimens.

Specimen	Peeling between skin and core (%)	Failure within core (%)	Delamination within skin (%)	Residue of carbon fibers on PLA core
0L-S10-1	34	66	0	Slight
0L-S10-2	100	0	0	Slight
0L-S5-1	90	0	10	Moderate
0L-S5-2	100	0	0	Slight
2L-S10-1	100	0	0	Moderate
2L-S10-2	0	100	0	N/A
2L-S5-1	100	0	0	Slight
2L-S5-2	80	0	20	Substantial

Per ASTM D1781, the average peeling load required to peel the adherend is to be calculated as an average of points from an autographic curve for 127 mm of peeling between 25 and 152 mm (1 and 6 in.). This corresponds to crosshead movement of 0.25 to 1.5 in. since head travel is converted to peeling distance by a factor of four [13]. For the eight specimens in this study, the average crosshead displacement at the start and the end of peeling was 29.2 and 60.6 mm, respectively. This 31.4 mm of head travel corresponds to a peeling distance of 125.6 mm.

Figure 10 (left) shows the average peeling load obtained for each specimen with an error bar representing the standard deviation for the sample. Here, standard deviation represents the variation in the load-extension data points (Figure 7) after the truncation point. 0L-S10-1 and 2L-S10-2 have the highest standard deviation and are the ones discussed earlier with the largest peaks and drops in the load-extension graphs among all the specimens. Average peeling load for all 0L specimens was 154 N with a coefficient of variation (CV) of 9.8% while it was 145 N for 2L specimens (CV: 8.2%). S10 and S5 specimens showed average peeling load of 157 N (CV: 6.6%) and 143 N (CV: 10.1%), respectively. This slightly higher consolidation strength for 0L and S10 specimens compared to the 2L and S5 samples contradicts what we expected in this study. A more detailed investigation of the consolidation strength including detailed micrograph analysis, other core materials, e.g., AM 200™, skin and core material compatibility, and higher number of specimens per each set should be completed as future work.

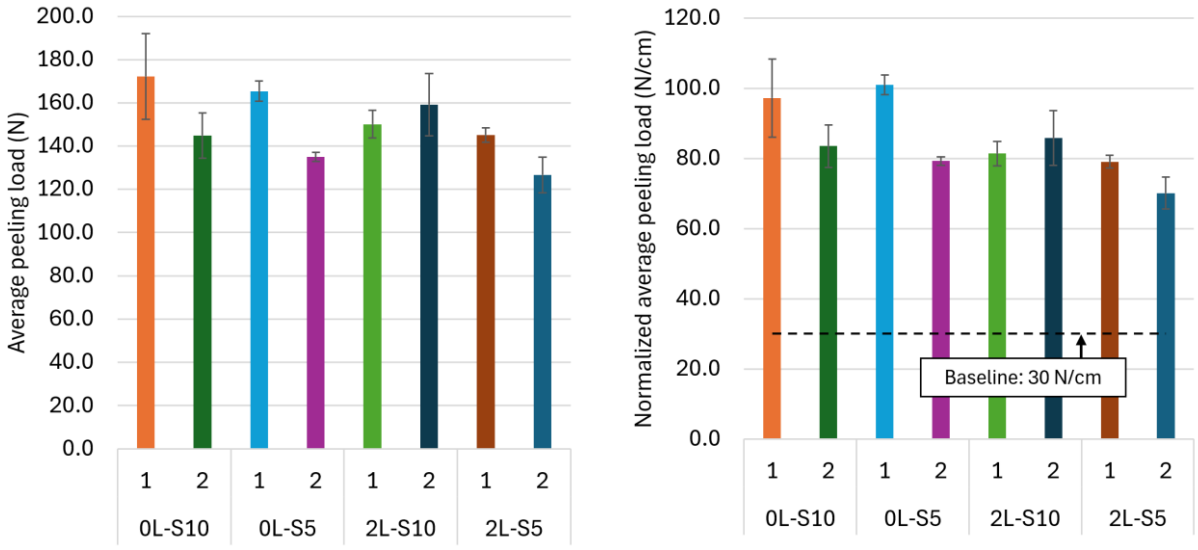

Figure 10. Average (left) and normalized peeling load (right) for thermoplastic sandwich specimens.

Next, the average peeling load was divided by the width of the peeled skin to normalize the results (Figure 10, right). Interestingly, the two specimens with failure within the core had the second and the third highest normalized peeling load. Therefore, while a PLA core was investigated in this study as a worst-case scenario for in-situ consolidation, its bulk properties were sufficient to investigate the peeling performance of the sandwich panels. This can be especially observed in specimen 0L-S10-1, which showed a combination of failure within the core and peeling between the skin and the core.

To the best of our knowledge, there is no prior study in the literature on 3D printed sandwich panels using the climbing drum peel test. Therefore, to compare our results with other manufacturing techniques of sandwich panels, we considered traditional fabrication techniques, e.g., hand layup and autoclave cure. The industrial partner of the project, Teijin Carbon America, provided a baseline of 30 N/cm for acceptable limits of the peeling load in aerospace applications. In addition, they shared test results for six composite sandwich specimens made from woven carbon fiber prepreg, resin film, and Kevlar honeycomb core, which had average normalized peeling load of 36.2 N/cm per EN2243-3. As it can be seen in Figure 10-right, all in-situ consolidated sandwich specimens exceeded the baseline of 30 N/cm by a factor greater than two. Therefore, this novel in-situ consolidation robotic 3D printing technique can manufacture high quality thermoplastic sandwich panels with skins from high-performance polymers reinforced with continuous carbon fiber without a film adhesive. It should be noted that the specimens in this paper are thermoplastic sandwich structures while the baseline was developed for thermoset composites. In general, thermoplastics are expected to have a higher fracture toughness than thermosets; therefore, a higher peeling load is expected. In future studies, thermoplastic sandwich specimens made using traditional fabrication techniques, e.g., hot press, should be compared with in-situ consolidated specimens of equivalent configuration. Tabulated data including average, maximum, and

minimum peeling load and normalized values for each individual specimen are provided in the data repository.

Linear-regression analysis was performed on the eight experimental data points using SigmaPlot 14.0. The normalized average peeling load as a function of the number of layers and the 3D printing speed was plotted with 95% confidence band (Figure 11). Note that a layer thickness of 0.2 mm was used for 3D printing the core; therefore, the number of pure PLA layers can be related to their thickness. The impact of the number of pure PLA layers on the normalized average peeling load is more significant than the 3D printing speed. Figure 11 (right) shows that higher 3D printing speed of 10 mm/s can be used without compromising the peeling load performance, leading to a higher production rate.

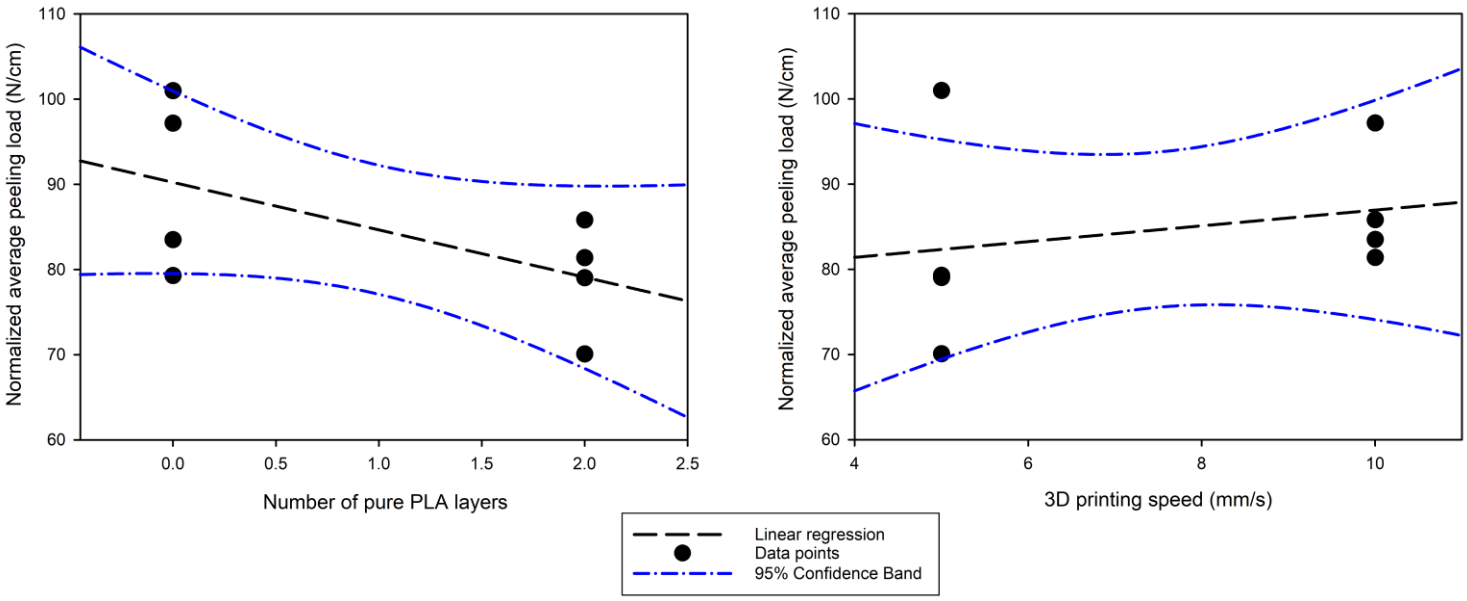

Figure 11. Normalized average peeling load as a function of the number of pure PLA layers (left) and the 3D printing speed (right).

Fiber pull-out and the carbon fiber residue left on the core proved sufficient consolidation between the skins and the core even though two dissimilar polymers, PLA and LM PAEK, were used. To investigate the interface between the skins and the core, a trial specimen with a core and no pure PLA layers was 3D printed at 10 mm/s (0L-S10). It was sectioned using a MECATOME T335 automatic cutting machine (Presi, Grenoble, France). A transparent epoxy resin with an eight-hour cure at room temperature was utilized to mount the sample, which was subsequently polished using a MECATECH 250 SPC automatic polisher from Presi. A VHX-X1 digital microscope (Keyence, Osaka, Japan) was used to create the micrograph of the whole sample (Figure 12).

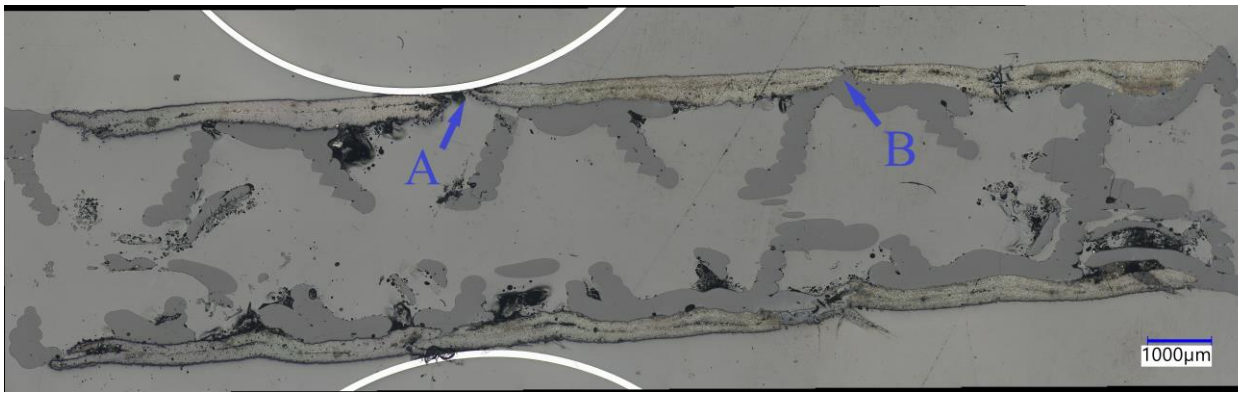

Figure 12. Micrograph of the trail sample, 0L-S10.

Figure 12 shows the top and bottom skins separated by the core with a complex geometry and no pure PLA layers. Proper consolidation between the two layers of each skin can be observed with two gaps (A and B) between the tapes of the top skin. These gaps were observed for 0L specimens in Figure 4, and the polymer squeeze-out, described in Figure 5, can be seen here as well (B). Note that the main objective of this research was to evaluate the integrity of in-situ consolidated sandwich panels with no film adhesive. To our knowledge, this is the first study to use the climbing drum peel test and to explore their peel performance. Further research is required to investigate the interface between the skins and the core using detailed micrographs to understand the mechanisms behind the consolidation strength of the panels. They can be due to the crystallization of LM PAEK and PLA, and the mechanical bonding between the skins and the core.

4. Conclusions

In this study, a novel in-situ consolidation robotic 3D printing method was proposed to fabricate thermoplastic sandwich specimens. Here, pure 20% gyroid poly lactic acid (PLA) cores were 3D printed using an Anycubic Kobra 2 max. Then, low-melt poly aryl ether ketone (LM PAEK) tapes reinforced with continuous carbon fiber (CCF) were deposited onto the core to make the sandwich specimens. They were tested according to a modified ASTM D1781 Standard Test Method for climbing drum peel for Adhesives. All combinations of the following two independent variables were explored for testing: (1) the integration of zero versus two pure PLA layers between skin and core, and (2) 10 mm/s versus 5 mm/s prepreg tape 3D printing speed. With two specimens per configuration, a total of eight specimens were fabricated and tested.

The thermoplastic sandwich specimens with two pure PLA layers between the skins and the core and 10 mm/s 3D printing speed had high quality facesheets with no gaps between individual tapes, higher surface finish, and no imprint from the core. There was no obvious trend between the core type or the 3D printing speed with the average peeling load of the specimens for the values selected in this paper. Therefore, a higher deposition speed of 10 mm/s can be utilized for an increased production rate without compromising the peeling load performance. The overall average force for all eight specimens was 150 N (CV: 9.6%). When normalized to the specimen's widths, the overall

average force-per-width was 84.7 N/cm (CV: 11.1%). This is a 182% increase from the baseline of 30 N/cm provided by the industrial partner for aerospace applications. Furthermore, this is equivalent to a 134% increase from average peeling load of 36.2 N/cm for six samples of two-layer woven carbon fiber prepreg, resin film, and Kevlar honeycomb core. These results validate in-situ consolidation robotic 3D printing as a potential fabrication method to produce sandwich structures from CCF LM PAEK without the need for film adhesive. This technique has many promises to reduce manufacturing cost and time, and increase recyclability of the final products. PLA was used as a worst-case scenario for in-situ consolidation, and it is expected that other thermoplastic cores, e.g., polyether ether ketone (PEEK), will provide greater improvements in peeling performance.

Sample width of about 18 mm in this paper complicated specimen clamping in the fixture, and a larger width is recommended for future studies. Furthermore, a comprehensive investigation of the consolidation strength including micrograph analysis, other core materials, and higher number of climbing drum peel samples should also be completed. Multi-scale, multi-physics computational modeling of the 3D printing technique and the climbing drum peel test can yield valuable insight into the in-situ consolidation process. It can be used to optimize the robotic 3D printing process parameters for maximum peeling performance. Since we validated this novel manufacturing technique here, it can now be used to deposit prepreg tapes onto thermoplastic parts with complex 3D geometries, e.g., concave and convex surfaces, to improve their structural performance.

Acknowledgments

The author would like to acknowledge Dr. Seyed Miri for his work on design and manufacturing of the 3D printing head. We would like to thank the industrial partner for the project, Teijin, for supplying the feedstock and Mr. Jean-Philippe Canart for his technical consultation.

Author contribution

Samuel Osorio Marino: Conceptualization, Data curation, Formal analysis, Investigation, Methodology, Visualization, Writing – original draft, Writing – review and editing. **Dalton Lamoureux:** Investigation, Methodology, Visualization, Writing – review and editing. **Kazem Fayazbakhsh**: Conceptualization, Funding acquisition, Project administration, Resources, Supervision, Writing – original draft, Writing – review and editing.

Funding

The financial support was provided by the Natural Sciences and Engineering Research Council of Canada (NSERC), RGPIN-2023-04091.

Data Availability

All information from this study, e.g., G-codes for all specimens, raw data from the testing machine, and dimensional measurements, is provided in the data repository (Mendeley Data, V2, doi: https://doi.org/10.17632/bkxcchbsxb.2).

References

[1] Qi, C., Jiang, F. and Yang, S., 2021. Advanced honeycomb designs for improving mechanical properties: A review. Composites Part B: Engineering, 227, p.109393.

[2] J. Jakobsen, E. Bozhevolnaya, and O. T. Thomsen, 'New peel stopper concept for sandwich structures', Compos Sci Technol, vol. 67, no. 15–16, pp. 3378–3385, Dec. 2007, doi: 10.1016/j.compscitech.2007.03.033.

[3] Ageorges, C., Ye, L. and Hou, M., 2001. Advances in fusion bonding techniques for joining thermoplastic matrix composites: a review. Composites Part A: applied science and manufacturing, 32(6), pp.839-857.

[4] K. F. Karlsson and B. T. Astrgm, 'Manufacturing and applications of structural sandwich components', 1997.

[5] P. R. Oliveira, M. May, T. H. Panzera, F. Scarpa, and S. Hiermaier, 'Improved sustainable sandwich panels based on bottle caps core', Compos B Eng, vol. 199, Oct. 2020, doi: 10.1016/j.compositesb.2020.108165.

[6] Li, T. and Wang, L., 2017. Bending behavior of sandwich composite structures with tunable 3D-printed core materials. Composite Structures, 175, pp.46-57.

[7] C. Lu et al., 'Mechanical performance of 3D-printing plastic honeycomb sandwich structure', International Journal of Precision Engineering and Manufacturing-Green Technology, vol. 5, no. 1, pp. 47–54, Jan. 2018, doi: 10.1007/s40684-018-0005-x.

[8] A. W. Alshaer and D. J. Harland, 'An investigation of the strength and stiffness of weight-saving sandwich beams with CFRP face sheets and seven 3D printed cores', Compos Struct, vol. 257, p. 113391, Feb. 2021, doi: 10.1016/j.compstruct.2020.113391.

[9] Sarvestani, H.Y., Akbarzadeh, A.H., Mirbolghasemi, A. and Hermenean, K., 2018. 3D printed meta-sandwich structures: Failure mechanism, energy absorption and multi-hit capability. Materials & Design, 160, pp.179-193.

[10] Peng, C., Fox, K., Qian, M., Nguyen-Xuan, H. and Tran, P., 2021. 3D printed sandwich beams with bioinspired cores: Mechanical performance and modelling. Thin-Walled Structures, 161, p.107471.

[11] H.-J. Um, J.-S. Lee, J.-H. Shin, and H.-S. Kim, '3D printed continuous carbon fiber reinforced thermoplastic composite sandwich structure with corrugated core for high stiffness/load capability', Compos Struct, vol. 291, p. 115590, Jul. 2022, doi: 10.1016/j.compstruct.2022.115590.

[12] K. Sugiyama, R. Matsuzaki, M. Ueda, A. Todoroki, and Y. Hirano, '3D printing of composite sandwich structures using continuous carbon fiber and fiber tension', Compos Part A Appl Sci Manuf, vol. 113, pp. 114–121, Oct. 2018, doi: 10.1016/j.compositesa.2018.07.029.

[13] ‘Test Method for Climbing Drum Peel for Adhesives’, Jun. 01, 2021, ASTM International, West Conshohocken, PA. doi: 10.1520/D1781-98R21.

[14] Miri, S., Kalman, J., Canart, J.P., Spangler, J. and Fayazbakhsh, K., 2022. Tensile and thermal properties of low-melt poly aryl ether ketone reinforced with continuous carbon fiber manufactured by robotic 3D printing. The International Journal of Advanced Manufacturing Technology, 122(2), pp.1041-1053.

[15] Y. Su, ‘Co-consolidation of titanium-C/PAEK joints: an investigation into the interfacial performance governing mechanisms’, University of Twente, 2016. doi: 10.3990/1.9789491909429.

[16] Z. Qureshi, T. Swait, R. Scaife, and H. M. El-Dessouky, ‘In situ consolidation of thermoplastic prepreg tape using automated tape placement technology: Potential and possibilities’, Compos B Eng, vol. 66, pp. 255–267, Nov. 2014, doi: 10.1016/j.compositesb.2014.05.025.

[17] S.-L. Gao and J.-K. Kim, ‘EFFECT OF COOLING RATE ON INTERPHASE PROPERTIES OF CARBON FIBRE/PEEK COMPOSITES’, Journal of the Society of Materials Science, Japan, vol. 48, no. 9 Appendix, pp. 157–162, 1999, doi: 10.2472/jsms.48.9Appendix_157.

[18] Gao, S.L. and Kim, J.K., 2000. Cooling rate influences in carbon fibre/PEEK composites. Part 1. Crystallinity and interface adhesion. Composites Part A: Applied science and manufacturing, 31(6), pp.517-530.

[19] Miri, S., Rana, J., Fayazbakhsh, K. and Ghnatios, C., 2025. Numerical and experimental study of the consolidation of continuous carbon fiber thermoplastics made by robotic 3D printing. International Journal of Material Forming, 18(1), p.1.

[20] Abedi, K., Miri, S., Gregorash, L. and Fayazbakhsh, K., 2022. Evaluation of electromagnetic shielding properties of high-performance continuous carbon fiber composites fabricated by robotic 3D printing. Additive Manufacturing, 54, p.102733.

[21] Rahimizadeh, A., Kalman, J., Fayazbakhsh, K. and Lessard, L., 2019. Recycling of fiberglass wind turbine blades into reinforced filaments for use in Additive Manufacturing. Composites Part B: Engineering, 175, p.107101.

[22] Bartlett, M., Anacreonte, A.V., Iasiello, M., Peracchio, A.A., Mauro, G.M., Bianco, N. and Chiu, W.K., 2024. An introduction to triply periodic minimal surfaces in thermal applications. In Thermopedia. Begel House Inc.

[23] F. Delfosse, ‘Gyroid infill in 3D printing: strength, efficiency, precision’. https://bigrep.com/posts/gyroid-infill-3d-printing/, 2025 (accessed 23 January 2026).

[24] García-Gascón, C., Castelló-Pedrero, P. and García-Manrique, J.A., 2022. Minimal surfaces as an innovative solution for the design of an additive manufactured solar-powered unmanned aerial vehicle (UAV). Drones, 6(10), p.285.

[25] ‘Preliminary Product Data Sheet Tenax ®-E TPUD PAEK-HTS45’, PLS 046 Rev A, February 4, 2020, ECCN 1C990, Teijin Carbon America, Inc., 121 Cardiff Valley Road, Rockwood, TN

37854. https://www.teijincarbon.com/products/thermoplastics/unidirectional-tapes/ (accessed 28 August 2025).